IVYSPRING INTERNATIONAL PUBLISHER

Theranostics

2018; 8(18): 4898-4911. doi: 10.7150/thno.27598

Research Paper

Two-stage oxygen delivery for enhanced radiotherapy by perfluorocarbon nanoparticles

Zaigang Zhou[1,2], Baoli Zhang[1,2], Haoran Wang[1,2], Ahu Yuan[1,2,✉], Yiqiao Hu[1,2,3,✉], Jinhui Wu[1,2,3,✉]

1. State Key Laboratory of Pharmaceutical Biotechnology, Medical School of Nanjing University & School of Life Sciences, Nanjing University, Nanjing 210093, China
2. Institute of Drug R&D, Nanjing University, Nanjing 210093, China
3. Jiangsu Provincial Key Laboratory for Nano Technology, Nanjing University, Nanjing 210093, China

✉ Corresponding authors: Jinhui Wu, Ph.D. Address: 22 Hankou Road, Nanjing University, Nanjing 210093, China. Phone: +86-25-83596143; Fax: +86-25-83596143; E-mail: wuj@nju.edu.cn, Yiqiao Hu, Ph. D. Address: 22 Hankou Road, Nanjing University, Nanjing 210093, China. Phone: +86-25-83596143; Fax: +86-25-83596143; E-mail: huyiqiao@nju.edu.cn and Ahu Yuan, Ph. D. Address: 22 Hankou Road, Nanjing University, Nanjing 210093, China. Phone: +86-25-83596143; Fax: +86-25-83596143; E-mail: yuannju@163.com

Received: 2018.06.01; Accepted: 2018.08.21; Published: 2018.09.09

Abstract

Tumors are usually hypoxic, which limits the efficacy of current tumor therapies, especially radiotherapy in which oxygen is essential to promote radiation-induced cell damage. Herein, by taking advantage of the ability of perfluorocarbon (PFC) to promote red blood cell penetration, we developed a simple but effective two-stage oxygen delivery strategy to modulate the hypoxic tumor microenvironment using PFC nanoparticles.

Methods: We first examined the two-stage oxygen delivery ability of PFC nanoparticles on relieving tumor hypoxia through platelet inhibition. To evaluate the effect of PFC nanoparticles on radiation sensitization, CT26 tumor and SUM49PT tumor model were used.

Results: In this study, PFC was encapsulated into albumin and intravenously injected into tumor-bearing mice without hyperoxic breathing. After accumulation in the tumor, PFC nanoparticles rapidly released the oxygen that was physically dissolved in PFC as the first-stage of oxygen delivery. Then, PFC subsequently promoted red blood cell infiltration, which further released O_2 as the second-stage of oxygen delivery.

Conclusion: The hypoxic tumor microenvironment was rapidly relieved via two-stage oxygen delivery, effectively increasing radiotherapy efficacy. The safety of all substances used in this study has been clinically demonstrated, ensuring that this simple strategy could be rapidly and easily translated into clinical applications to solve the clinical problems associated with tumor hypoxia.

Key words: perfluorocarbon nanoparticles, tumor hypoxia, two-stage oxygen delivery, radiotherapy

Introduction

Hypoxia resulting from abnormal tumor blood vessels, excessive tumor cell proliferation and an aberrant lymphatic system is a common malignant phenomenon in almost all solid tumors [1, 2]. According to previous research, tumor hypoxia has been shown to be one of the vital causes of tumor therapy failure [1, 3]. In particular, for radiotherapy, oxygen is the essential element for generation of the reactive oxygen species that kill tumors [4]. Therefore, the hypoxic tumor microenvironment is often a vital cause of radiotherapy resistance.

Recently, different strategies have been proposed to reverse tumor hypoxia and obtain better radiotherapy outcomes, but still, no good oxygen donor is yet available for clinical use to relieve tumor hypoxia [5-7]. In particular, although hyperoxic breathing can increase the sensitivity of tumor therapy by increasing the oxygenation status of systemic cells, the apparent side effects, such as lung injury and neurotoxicity, would significantly limit its clinical application [8, 9]. In addition, due to its good chemical oxygen-carrying capacity, hemoglobin is also widely used to relieve tumor hypoxia, but it can cause acute nephrotoxicity and acute hypertension, which pose a serious threat to patient lives [10, 11]. Currently, tumor environment-responsive oxygen

delivery strategies, such as manganese dioxide, have also been shown to be effective in reversing hypoxic tumors to a certain extent [5, 12]. However, the tumor re-oxygenation levels achieved by this method are still seriously restricted by the limited amount of H_2O_2 in the tumor surroundings and the toxicity to normal cells of Mn^{2+} itself [13]. Other methods, such as normalizing tumor vessels or reducing tumor interstitial pressure via enzymes, can also effectively reverse tumor hypoxia to a certain extent [14, 15]. Nevertheless, the obvious drawbacks of normalizing tumor vessels, including the narrow effective dosage window and enhanced tumor metastasis, limit its wide use [16, 17]. Therefore, the search for more effective oxygen carriers for relief of tumor hypoxia has become an urgent problem.

PFCs, a group of chemically inert synthetic molecules with excellent biocompatibility, have been widely studied or used in the clinic for various purposes, including artificial blood substitution, organ preservation, ultrasound imaging and fluorine magnetic imaging [18-20]. More importantly, due to their high oxygen solubility, PFCs have been extensively explored as oxygen suppliers to increase the therapeutic outcome of radiotherapy or photodynamic therapy [13, 21-23]. However, the effectiveness of this strategy is still limited because the release of oxygen dissolved in PFCs occurs only by simple diffusion according to the oxygen concentration gradient, which is inefficient and needs to be triggered by external stimulus, such as near-infrared light laser or ultrasound [13, 24-27].

Currently, directly increasing the number of red blood cells at the tumor site is one of the most effective ways to relieve tumor hypoxia [28]. Increasing evidence has shown that platelet inhibition could increase tumor blood vessel permeability, which in turn enhances red blood cell infiltration and promotes O_2 delivery at tumor sites [29, 30]. PFC has been studied as a blood substitute for more than half a century. However, one phenomenon that has been neglected is that PFC itself has platelet inhibition capability, which might be used to increase red blood cell infiltration into tumors and thus improve the O_2 supply in tumors [31].

Through screening, we found that perfluorotributylamine (PFTBA) possessed the strongest platelet inhibition effect of all the perfluorocarbon compounds. Therefore, in this study, we took advantage of the platelet inhibition effect of PFTBA to establish a two-stage O_2 delivery system (PFTBA@HSA) by using albumin as a carrier (**Figure 1**). After intravenous injection, PFTBA@HSA nanoparticles accumulated at the tumor site due to the EPR effect and released its physically bound O_2 (1st stage oxygen supply). At the same time, PFTBA effectively inhibited platelet activation in the tumor blood vessels to disrupt well-maintained tumor vessel barriers, which then lead to an increase in RBCs (red blood cell) infiltration and oxygen delivery by RBCs in the tumor (2nd stage oxygen supply). Our work presents a simple but effective method to reverse the resistance of tumor hypoxia to radiotherapy. This technique shows great promise for future clinical translation since all agents, including PFTBA and albumin, are readily available in the clinic and have been verified as nontoxic.

Methods

Chemicals and reagents

PFTBA and PPA (perfluorotripropylamine) were acquired from Silworld Chemical Co. Ltd. (Wuhan, China). HSA (human serum albumin) was purchased from CSL Behring AG (Switzerland). Evans Blue dye was obtained from Aladdin Industrial Corporation (Shanghai, China). CT26 cells and SUM149PT cells were acquired from the Cell Bank of Shanghai Institutes for Biological Sciences, Chinese Academy of Sciences (Shanghai, China). Balb/C mice were purchased from Yangzhou University Medical Centre (Yangzhou, China).

Synthesis and characterization of PFTBA@HSA nanoparticles

In general, 96 mg HSA and dithiothreitol were dissolved in 2.4 mL deionized water, followed by stirring for 10 min. Then, 200 μL alcohol was added to the solution, followed by shaking for another 3 min. Finally, 0.6 mL PFTBA or 0.48 mL PPA and 0.12 mL FDC (perfluorodecalin) were injected under 300 W sonication (Xokeji, XO-650D, China) for 6 min in an ice bath to form PFTBA@HSA or PPA@HSA nanoparticles. The size of the PFC@HSA nanoparticles was determined by dynamic light scattering (DLS, 90Plus, Brookhaven Instrum. Corp). The morphology and structure of the PFTBA@HSA nanoparticles were characterized via transmission electron microscopy (TEM, JEM-2100, Japan). The stability of PFTBA@HSA in H_2O, PBS and Plasma was evaluated by size determination.

Platelet-rich plasma preparation

The blood of Balb/C male mice was collected into centrifuge tubes containing moderate sodium citrate. The blood was centrifuged at 203 ×*g* for 10 min to collect PRP (platelet-rich plasma). After addition of 125 ng/mL PGI_2, the PRP was further centrifuged at 1028×*g* for 5 min. Platelets in the bottom of the centrifuge tubes were re-suspended in modified Tyrodes-HEPES buffer (134 mM NaCl, 2.9 mM KCl,

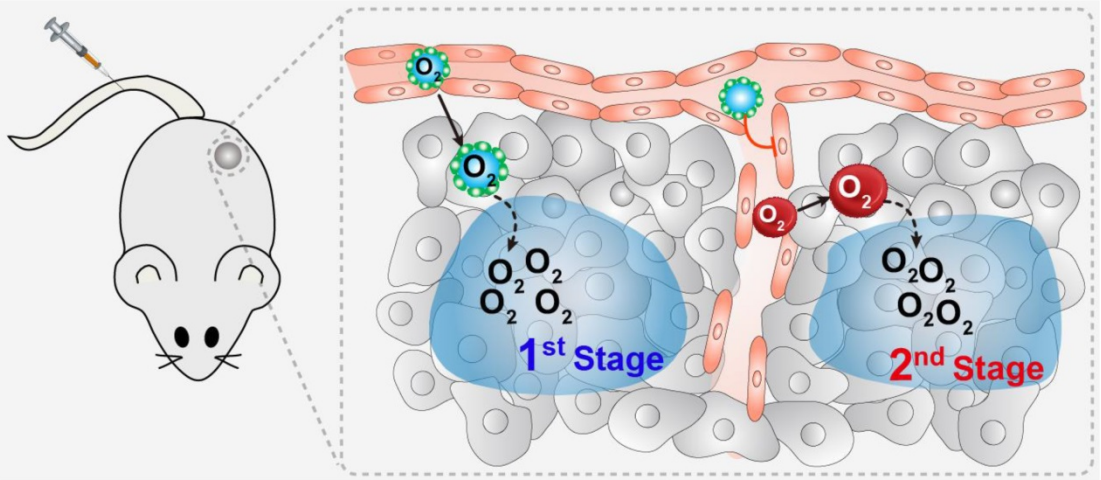

Figure 1. Schematic illustration of the two-stage oxygen delivery system. After intravenous injection, PFTBA@HSA nanoparticles accumulate at the tumor site due to the EPR effect and release physically bound O_2 (1st stage oxygen supply). At the same time, PFTBA could effectively inhibit platelet activation in the tumor blood vessels to disrupt well-maintained tumor vessel barriers, which then leads to increased RBCs (red blood cell) infiltration and oxygen delivery by RBCs in the tumor (2nd stage oxygen supply).

0.34 mM $Na_2HPO_4.12H_2O$, 12 mM $NaHCO_3$, 20 mM HEPES and 1 mM $MgCl_2$, pH 7.3) to a final density of 4×10^8 cells/mL for further assays.

Clot retraction assay

Platelets were prepared as mentioned previously. The platelets (4×10^8 cells /mL) were mixed with 50 μL Vehicle (32 mg/mL HSA) or 50 μL PFTBA@HSA. The solution was adjusted to 1 mL with modified Tyrodes-HEPES buffer, followed by addition of 5 μL red blood cells. Fibrin clot formation was initiated by addition of 5 μL thrombin (200 U/mL). Finally, a glass capillary was added. Clot formation and retraction were observed over a period of 90 min at 37 ℃. Clot weight and extruded serum weight were measured as markers for clot retraction.

Platelet aggregation assay

The platelet aggregation assay was performed and detected using UV microplate reader at 650 nm in the presence or absence of PFTBA@HSA. Generally, 60 μL PRP was prepared and incubated with 12 μL PFTBA@HSA or Vehicle (32 mg/mL HSA) for 30 min at 37 ℃. Then, 5 μL thrombin (200 U/mL) was added to activate the platelets. The ultraviolet absorption at 650 nm was detected before and after thrombin addition. Platelet aggregation rates were calculated as follows: platelet aggregation rate (%) = $(1 - Abs_{thrombin}^{+} / Abs_{thrombin}^{-}) \times 100\%$, where $Abs_{thrombin}^{-}$ represents the ultraviolet absorption of platelet solution at 650 nm before thrombin addition, and $Abs_{thrombin}^{+}$ represents the ultraviolet absorption of platelet solution at 650 nm after addition of thrombin.

ATP secretion assay

ATP secretion assays were performed through luminescence aggregometry using luciferase luminescence substrate. In general, 60 μL PRP was prepared as mentioned previously via co-incubation with 12 μL PFTBA@HSA or Vehicle for 30 min at 37 ℃. Then, 5 μL thrombin (200 U/mL) was added to activate the platelets. The ATP secreted from washed platelets was measured according to the luminescence level.

Oxygen-carrying capability of PFTBA@HSA

4 mL of as-prepared PFTBA@HSA nanoparticles or Vehicle (32 mg/mL HSA) was stored in an aseptic oxygen chamber (O_2 flow rate = 5 L/min) for 1 min for PFCs oxygenation. The oxygen concentrations were measured using Unisense™ oxygen probe.

Cells and tumor models

CT26 cells were cultured with RPMI 1640 medium supplemented with 10% fetal calf serum and 1% 200 mM L-glutamine. SUM149PT cells were cultured with DMEM supplemented with 10% fetal calf serum and 1% 200 mM L-glutamine.

All animal tests and experimental procedures were approved by the Administration Committee of Experimental Animals in Jiangsu Province and the Ethics Committee of Nanjing University. The animals were housed with free access to food and water.

To establish CT26 tumor-bearing mice, the hair on the right flank of the mice was removed. Male Balb/C mice subcutaneous tumor models were established by subcutaneous injection of 1×10^6 CT26 cells into the mice. Tumors were collected and cut into small pieces (~2 mm^3) when the tumor volume grew to approximately 150 mm^3. The tumor pieces were subcutaneously implanted into other mice to establish CT26 tumors. To establish the SUM149PT tumor model, SUM149PT cells (4×10^6 cells in 100 μL DMEM, 50% Matrigel) were implanted into the second

abdominal mammary pads of the Balb/C female mice.

Quantification of intra-tumor hemoglobin

Generally, CT26 tumors bearing mice were selected and treated with Vehicle or PFTBA@HSA (10 mL/kg). 1 h, 5 h or 10 h later, the mice were sacrificed to collect tumors. Then, these tumors were homogenized in Drabkin's reagent (Sigma) for 24 h at room temperature, followed by centrifugation at 15000 ×*g* for 10 min. The hemoglobin concentration of the supernatants was measured by using absorbance at 540 nm via UV-VIS spectrophotometry (Shimadzu).

In vivo hypoxia assessment

For HIF-1α-based hypoxia detection, 10 mL/kg PFTBA@HSA nanoparticles, 10 mL/kg PPA@HSA nanoparticles or Vehicle were intravenously injected into CT26 tumor-bearing mice (~200 mm^3) to research the effects of PFC@HSAs' medicated two-stage oxygen delivery on relieving tumor hypoxia. At 12 h or 24 h later, the mice were sacrificed to collect the tumors, embedded into OCT and cut into 8 μm slices. Tumor sections were incubated with Alexa-Fluor 488-labeled anti-mouse HIF-1α antibody (dilution 1:200, Thermal Fisher Inc.) at 4 ℃ overnight. The tumor cell nuclei were stained with DAPI for 5 min. Finally, fluorescence images of the slices were observed via fluorescence microscopy (Nikon, Japan).

For HIF-1α-based hypoxia detection, 10 μL PFTBA@HSA nanoparticles, 10 μL PPA@HSA nanoparticles or Vehicle were intratumorally injected into CT26 tumor-bearing mice (~200 mm^3) to research the effects of PFC@HSAs' physically bound oxygen-mediated one-stage oxygen delivery on relieving tumor hypoxia. After 12 h, the mice were sacrificed, embedded into OCT and cut into 8 μm slices. Tumor sections were incubated with Alexa-Fluor 488-labeled anti-mouse HIF-1α antibody (dilution 1:200, Thermal Fisher Inc.) at 4 ℃ overnight. Tumor cell nuclei were stained with DAPI for 5 min. Finally, fluorescence images of the slices were observed via fluorescence microscopy (Nikon, Japan).

For Pimonidazole-based hypoxia detection, 10 mL/kg PFTBA@HSA nanoparticles, 10 mL/kg PPA@HSA nanoparticles or Vehicle were intravenously injected into CT26 tumor-bearing mice (~200 mm^3) to research the effects of PFC@HSAs-mediated two-stage oxygen delivery on relieving tumor hypoxia. 3 hours later, 90 mg/kg Pimonidzole was given through tail vein injection after different treatments. After 12 h or 24 h, the mice were sacrificed, embedded into OCT and cut into 8-μm slices to detect the Pimonidazole accumulation levels. Tumor sections were incubated with FITC-labeled rat anti-mouse Pimonidazole antibody (dilution 1:200, HPI.) at 4 ℃. The tumor cell nuclei were stained with DAPI for 5 min. Finally, fluorescence images of the slices were observed via fluorescence microscopy (Nikon, Japan).

For Pimonidazole-based hypoxia detection, 10 μL PFTBA@HSA nanoparticles, 10 μL PPA@HSA nanoparticles or vehicle were intratumorally injected into CT26 tumor-bearing mice (~200 mm^3) to research the effects of PFC@HSAs' physically bound oxygen-mediated one-stage oxygen delivery on relieving tumor hypoxia. 3 hours later, 90 mg/kg Pimonidzole was given through tail vein injection after different treatments. After another 12 h, the mice were sacrificed, embedded into OCT and cut into 8-μm slices to detect Pimonidazole accumulation levels. Tumor sections were incubated with FITC-labeled rat anti-mouse Pimonidazole antibody (dilution 1:200, HPI) at 4 ℃. The tumor cell nuclei were stained with DAPI for 5 min. Finally, fluorescence images of the slices were observed via fluorescence microscopy (Nikon, Japan).

In vivo combination radiotherapy in a CT26 tumor model

Balb/C mice bearing subcutaneous CT26 tumors (~50 mm^3) were randomly divided into four groups (n=5): (1) Vehicle (32 mg/mL HSA, 10 mL/kg); (2) PFTBA@HSA nanoparticles (10 mL/kg); (3) PPA@HSA nanoparticles (10 mL/kg); (4) 5 Gy irradiation; (5) PFTBA@HSA nanoparticles (10 mL/kg) co-treated with 5 Gy radiation (6) PPA@HSA nanoparticles (10 mL/kg) co-treated with 5 Gy radiation. The mice were treated with radiation therapy 10 h after PFTBA@HSA or PPA@HSA pretreatment. The treatments or drugs were administered at day 0 and day 4 via tail vein injection. Calipers were used to measure the tumor volume, which was calculated as follows: $a \times b^2 \times 0.5$, where a represents the length of tumor, and b represents the width of the tumor. At the 14^{th} day, the tumors were removed by dissection, followed by tumor weighing and imaging.

Some of the tumors and major organs were collected 24 h after the various treatments. H&E staining, Tunel (terminal deoxynucleotidyl transferase dUTP nick end labeling) immunohistochemical staining and γH_2AX immunohistochemical staining were used to stain the tumor slices. For H&E staining, the 8-μm paraffin slices were stained with H&E, and images were acquired with a digital microscope (Nikon, Japan). For the Tunel assay, Tunel staining was applied following the instructions of *In situ* Cell Death Detection kit (Roche, USA).

In vivo combination radiotherapy in the SUM149PT tumor model

Balb/C nude female mice bearing subcutaneous SUM149PT tumors (~200 mm^3) were randomly divided into four groups (n=6): (1) Vehicle (32 mg/mL HSA, 10 mL/kg); (2) PFTBA@HSA nanoparticles (10 mL/kg); (3) 2 Gy radiation; or (4) PFTBA@HSA nanoparticles (10 mL/kg) combined with 2 Gy radiation 10 h later. Vehicle or PFTBA@HSA was given via tail vein injection. These drugs or treatments were administered given twice every week. Calipers were used to measure tumor volume, which was calculated as follows: $a \times b^2 \times 0.5$, where a represents the length, and b represents the width of the tumor.

The experiment was stopped on the 25th day, and the tumors were removed by dissection followed by tumor weighing. H&E, TUNEL and γH_2AX staining were used to stain the tumor slices to detect the efficacy of these treatments. The tumors and normal tissues were collected on the 25th day. For H&E staining, the slices were stained with H&E, and images were acquired with a digital microscope (Nikon, Japan). For the TUNEL assay, fluorescent TUNEL staining was applied following the instructions of the *In situ* Cell Death Detection kit (Roche, USA).

Statistical analysis

Data are presented as the mean ± SD. Statistical analysis was performed via one-way ANOVA test. Meanwhile, post hoc analysis was performed using the Wilcoxon rank sum test with a Bonferroni correction if needed. *p<0.05 was considered statistically significant, **p<0.01 and ***p<0.001 were considered extremely significant.

Results

Synthesis and characteristics of PFTBA@HSA

Since PFCs are very hydrophobic, they must be prepared with hydrophilic nanoparticles for intravenous injection. In this study, albumin was chosen as the drug carrier to encapsulate perfluorocarbon into nanoparticles using our previously developed "unfolding self-assembly" method (**Figure 2A**) [32, 33]. Briefly, the hydrophobic regions of albumin were first exposed by cutting off disulfide bonds and then self-assembled with perfluorocarbon to form nanoparticles. The average size of PFTBA@HSA was approximately 150 nm with a PDI of 0.0846, as determined by dynamic light scattering (DLS) (**Figure 2B**). Using transmission electron microscopy (TEM), PFTBA@HSA was found to exhibit a uniform size distribution, which is consistent with the DLS data (**Figure 2C**). The zeta potential was approximately -35 mV, indicating excellent stability in aqueous solution (**Figure S1**). After mixing with H_2O, PBS or Plasma, the mean particle size of PFTBA@HSA was constant for at least 24 h (**Figure 2D**). In addition, cell viability test revealed that PFTBA@HSA showed no toxicity on tissue cells, including normal cells and tumor cells (**Figure S2**). The oxygen-carrying and oxygen-release capabilities of PFTBA@HSA were evaluated using an oxygen meter to measure the dissolved oxygen concentration in aqueous solution [26, 34, 35]. The dissolved oxygen concentration in PFTBA@HSA at 25 °C under 1 atm was approximately 500 μM [13], which is consistent with results reported in the literature (**Figure 2E**).

Effects of PFTBA@HSA on platelet function and RBC infiltration

Recent reports have indicated that platelets play an important role in maintenance of tumor vessel integrity by secreting active ingredients, such as serotonin and angiogenin-1[36]. Platelet inhibition can effectively decrease endothelial cell numbers, destroy endothelial cell arrangements and reduce endothelial cell tight junctions [37, 38]. Therefore, blocking of platelets can destroy tumor vessel integrity, causing increased RBC infiltration into the tumor and enhancing tumor oxygenation.

The oxygen-loading ability of PFCs has been widely studied, and PFCs have been clinically used as blood substitutes. Although PFCs are chemically inert, they might adversely affect blood platelets, resulting in thrombocytopenia [39, 40]. Thus, we screened a series of PFCs through clot retraction assay and found that PFTBA possessed the most obvious inhibition effect on platelet function (**Figure S3**). For this reason, we used PFTBA as the main oxygen donor in this study to construct the nanoparticles. The inhibition effect of PFTBA@HSA on platelets was studied in the presence of thrombin because thrombin can effectively induce platelet activation and aggregation (**Figure 3A**). After addition of PFTBA@HSA, thrombin-induced platelet activation was obviously inhibited (**Figure 3A-C**). Finally, the blood was completely coagulated, and the fibrin network shrunk due to the action of the platelet thrombin-contracting protein, which caused the serum to precipitate and the blood clot to shrink. The degree of contraction was closely related to the quantity and function of the platelets (**Figure 3D**). In the presence of PFTBA@HSA, the shrinkage of blood clots was significantly inhibited, which resulted in an increase in blood clot weight and reduced serum release (**Figure 3E-F**). Thus, PFTBA@HSA possessed

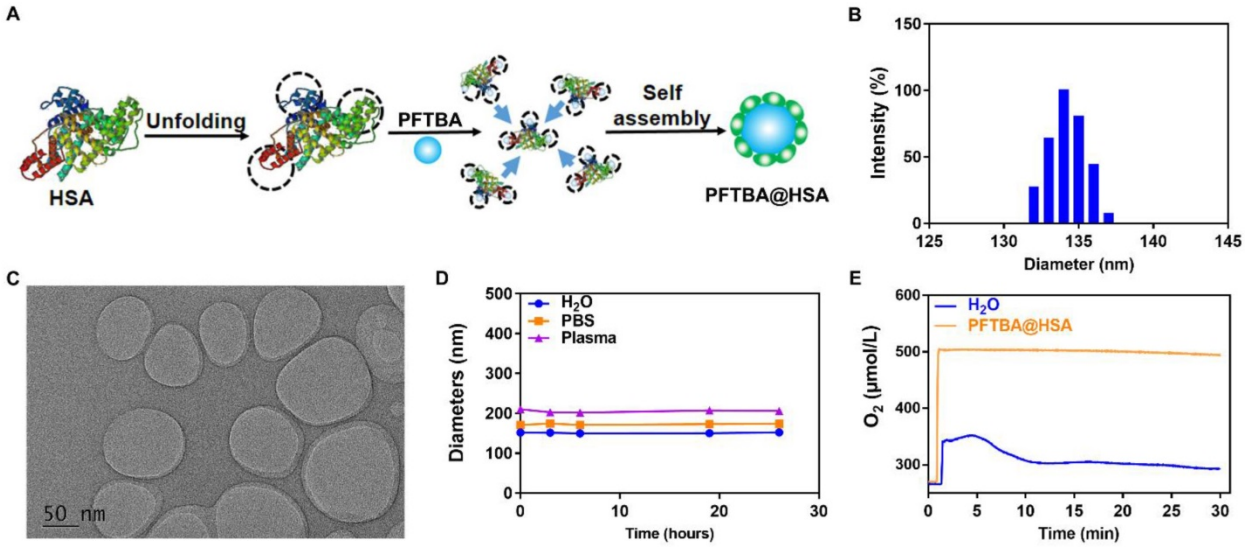

Figure 2. Synthesis and characteristics of PFTBA@HSA. (A) 'Unfolding self-assembly' method. Briefly, hydrophobic regions of albumin were first exposed by cutting off disulfide bonds followed by self-assembly with perfluorocarbons to form PFTBA@HSA nanoparticles. **(B)** PFTBA@HSA diameters detected via dynamic light scattering. **(C)** TEM images of PFTBA@HSA. **(D)** Stability of PFTBA@HSA mixed with different solutions: H_2O, PBS and plasma. **(E)** The oxygen release profile of O_2-adsorbed PFTBA@HSA under 1 atm. Data are shown as mean ± SD.

good platelet inhibition capability. In fact, previous research showed that PFC may absorb onto the surface of the cell membrane [41]. We used energy dispersive spectrometry and TEM to evaluate the concentration of fluorine in the platelet membranes. The results showed that some fluorine from PFTBA@HSA exists on the surface of platelets. Thus, we thought that the platelet activation pathway or membrane glycoprotein may be effectively covered by PFTBA@HSA, which may lead to platelet inhibition (**Figure S4**).

Many recent studies have demonstrated that platelets play an important role in maintenance of tumor vessel integrity. Thus, we speculated that inhibition of platelets by PFTBA@HSA could disrupt blood vessel integrity and increase RBCs penetration at the tumor site. We first used Evans Blue dye to study the effect of PFTBA@HSA on blood vessel integrity. Results showed that the permeability of blood vessels to Evans Blue was significantly increased by PFTBA@HSA administration to tumor-bearing mice (**Figure S5**). We also studied RBC infiltration into tumor tissue at 1, 5, and 10 h after PFTBA administration. The results revealed that the number of RBCs within the tumor was significantly increased at 5 and 10 h after PFTBA@HSA administration (**Figure 3G-H**). Additional platelet administration inhibited the increase in the number of red blood cells (**Figure 3G**). These findings showed that the effects of PFTBA@HSA on increasing RBCs infiltration in the tumor were at least partially directed by platelet inhibition (**Figure 3G**). As we deduced, increased RBCs infiltration further increased the supply of O_2 in the tumor to improve the oxygen partial pressure in the tumor. More interestingly, PFTBA@HSA had no effect on the hemoglobin content or RBCs infiltration in normal tissues, including the heart, liver, spleen, lung and kidney (**Figure S6**). In tumor, vascular endothelial cells are fewer and irregularly arranged. Abundant inflammatory factors are abnormally expressed in the tumor, leading to reduced endothelial cell tight junctions and increased endothelial cell damage [36, 42-44]. However, in the normal blood vessel, endothelial cells are more abundant and in a state of dense connection. These well-arranged endothelial cells do not need activation of platelets to maintain the integrity of blood vessels [36, 42-44]. Thus, platelets inhibition has no effect on the hemoglobin content or RBCs infiltration in normal tissues. Together, these results indicate that PFCs can selectively inhibit platelets in tumor vessels.

Reversal of tumor hypoxia via two-stage oxygen delivery by PFTBA@HSA

To further demonstrate the selectivity of PFTBA@HSA for platelet inhibition in tumors, IR775 was loaded into PFTBA@HSA for near-infrared (NIR) imaging. IR-775-labeled PFTBA@HSA nanoparticles were found to primarily accumulate in the tumor site after intravenous injection and thus showed significant tumor targeting capacity. The preferential accumulation in tumors might be due to the enhanced permeability and retention (EPR) effect and active tumor cell targeting due to high SPARC (secreted protein acidic and rich in cysteine) expression on the tumor cell membrane (**Figure S7**). Meanwhile, the accumulation of PFTBA in tumor was determined by

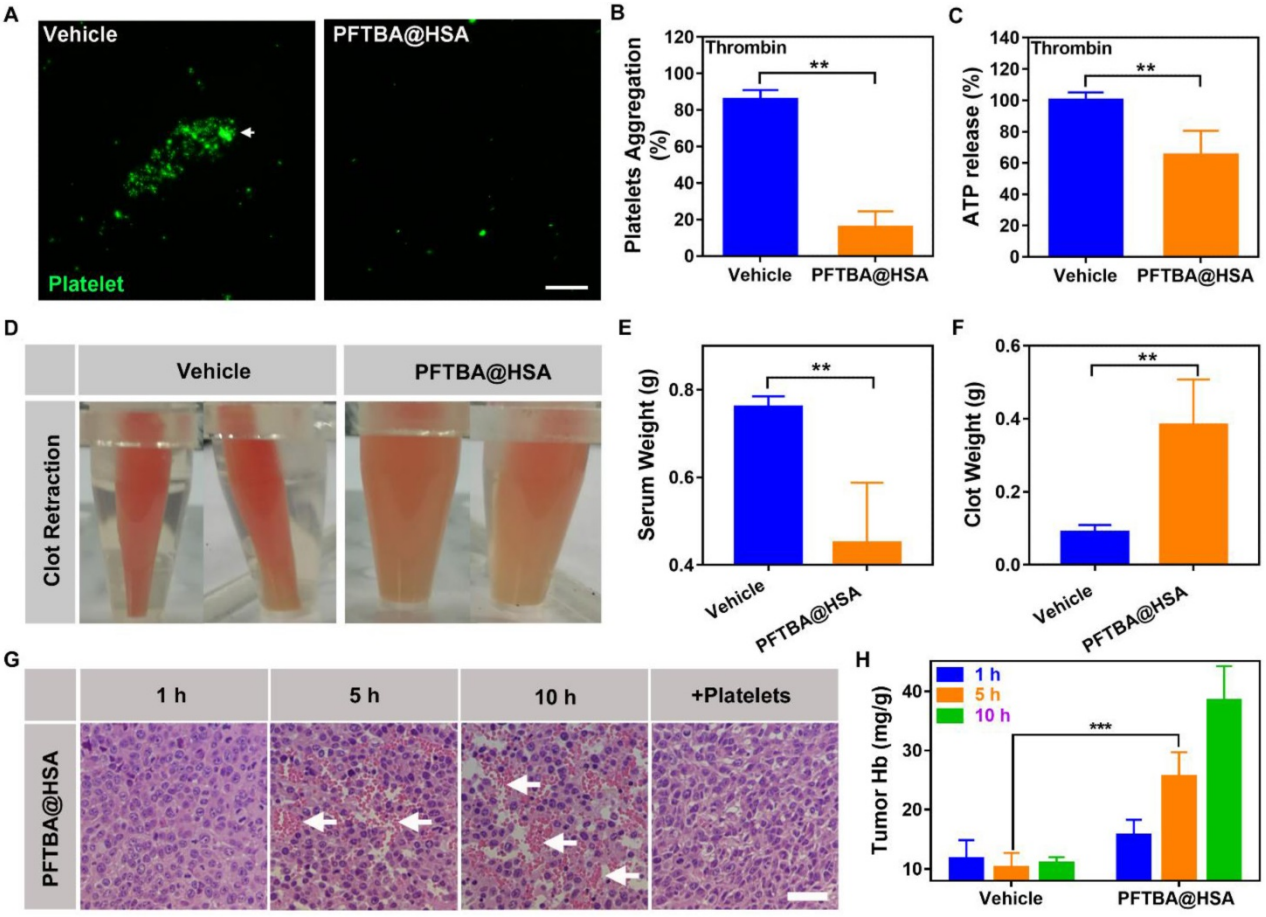

Figure 3. Effects of PFTBA@HSA on platelet function and RBCs infiltration. (A) Representative image of platelet aggregation activated by thrombin in the presence of vehicle or PFTBA@HSA. White arrows denote the position of platelet aggregation; scale bar = 50 μm. **(B)** Platelet aggregation induced by thrombin. The data were calculated as the absorbance ratio before and after activation (n=6). **(C)** ATP release from platelets activated by thrombin (n=6). **(D)** Representative photos of clot retraction. **(E)** Quantification of serum weight (n=8). **(F)** Quantification of clotting weight (n=8). **(G)** H&E staining of PFTBA@HSA-treated tumor slices at different times. White arrows denote RBCs; scale bar = 25 μm. **(H)** Quantification of hemoglobin after vehicle or PFTBA@HSA administration (n=6). Data are shown as the mean ± SD. Statistical analysis was performed via one-way ANOVA test. **p<0.01; ***p<0.001.

gas chromatography (**Figure S8**). It reached its maximum at 48 h, which was consistent with the results detected by NIR imaging. These results indicated that nanoparticles were highly accumulated at the tumor site at 48 h post-injection. All these results in our study indicated that PFTBA@HSA can achieve high accumulation in the tumor.

PFCs have been demonstrated to be good O_2 carriers and can release O_2 at low oxygen partial pressures [45, 46]. Due to tumor hypoxia, O_2 was released by free diffusion from PFTBA@HSA when the nanoparticles circulated to the tumor tissue site, namely, the first-stage oxygen release. In this study, PPA@HSA was used as an ideal control in these studies as one-stage oxygen delivery with only physically bound oxygen. The results showed that PPA@HSA (~160 nm) obtained similar nanoscale and shape as PFTBA@HSA (~150 nm) (**Figure S9**). Meanwhile, the oxygen solubility of PPA@HSA (~480 μM) was also similar to that of PFTBA@HSA (~500 μM) (**Figure S10**). We found that tumor hypoxia was obviously relieved at 5 h after intratumoral injection of PFC@HSAs, as indicated by Pimonidazole (**Figure 4A-B**). However, PFTBA@HSA was unable to relieve tumor hypoxia over a long period because no difference in HIF-1α staining or Pimonidazole accumulation was observed 12 h after treatments (**Figure 4A-E**). Meanwhile, the western blot analysis of HIF-1α also proved that PFTBA@HSA could not effectively relieve hypoxia for a long period after intratumoral injection (**Figure 4F-G**). Therefore, oxygen supplied by PFC@HSA itself (1st stage oxygen delivery) was not sufficient to relieve long-term tumor hypoxia, which significantly limited its potential clinical usage.

Interestingly, we had previously demonstrated that PFTBA@HSA was able to increase RBCs infiltration at the tumor site. The increase in the number of red blood cells at the tumor site would likely endow PFTBA with second-stage oxygen release capability (**Figure S11**). To validate this hypothesis, we evaluated the two-stage oxygen

delivery effects of PFTBA@HSA on relieving tumor hypoxia via tail vein injection. Results showed that the HIF-1α expression in the tumor cells was significantly decreased at both 12 and 24 h after PFTBA@HSA treatment (**Figure 5A-C** and **Figure S12**). Meanwhile, the western blot analysis of HIF-1α also proved that PFTBA@HSA could effectively relieve hypoxia for a long period via two-stage oxygen delivery realized by platelet inhibition-mediated enhanced RBCs infiltration in tumor and dissolving of physical oxygen (**Figure 5D-E**). Moreover, the accumulation of another hypoxia indicator (Pimonidazole) in the tumors showed results similar to those obtained with HIF-1α assessment (**Figure 5F-H**). However, PPA@HSA did not exhibit the same effect on relieving long-term tumor hypoxia after tail vein administration (**Figure 5**), although its structure is similar to that of PFTBA. This result might be due to the fact that PPA@HSA did not show the inhibitory effect on platelets that PFTBA@HSA possessed (**Figure S3**). Therefore, our well-designed two-stage PFTBA@HSA oxygen delivery system simultaneously relieved short-term and long-term tumor hypoxia.

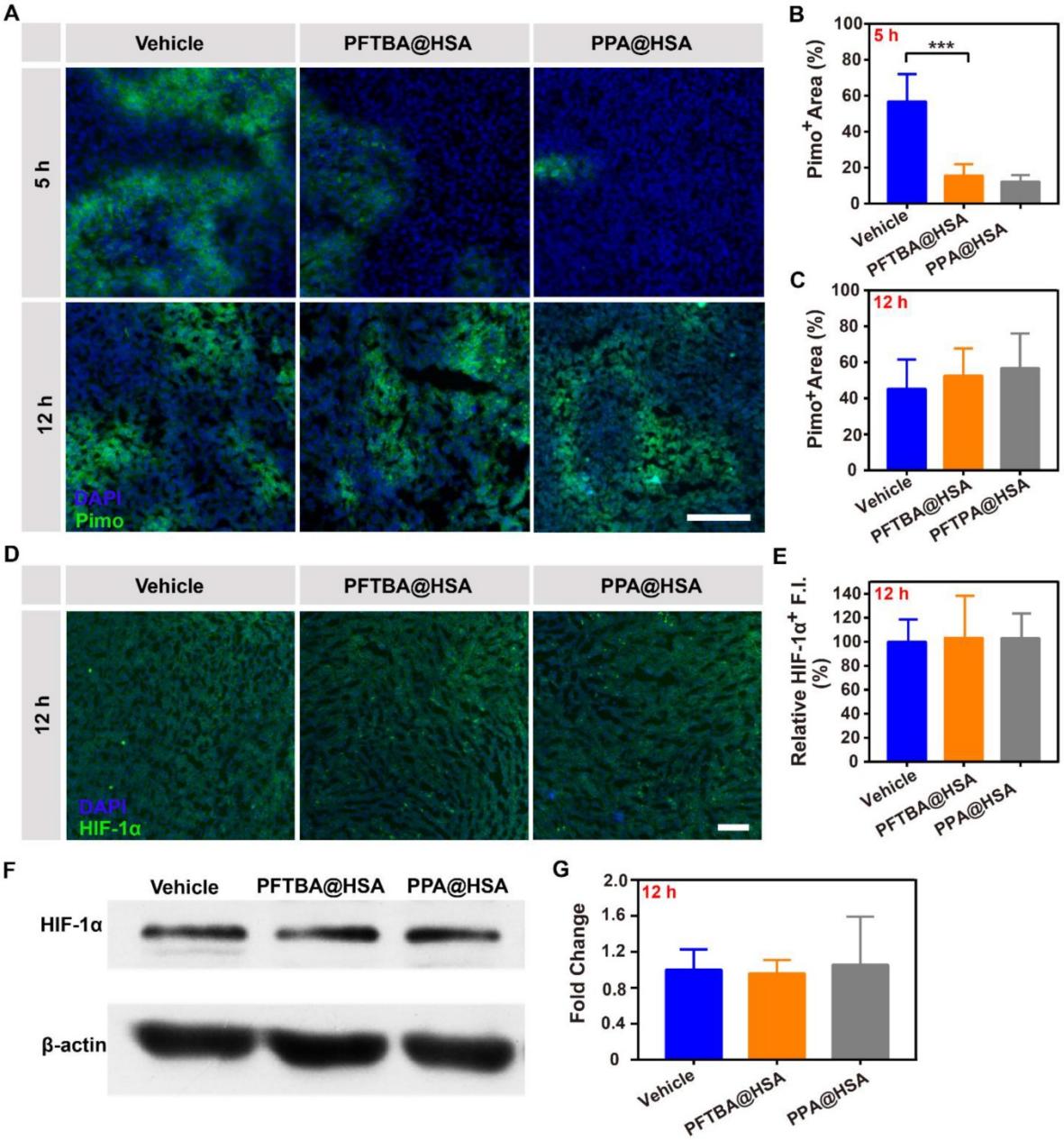

Figure 4. Effects of PFTBA@HSA on relief of CT26 tumor hypoxia after intratumoral injection. (A) Representative immunofluorescence images of tumor slices stained with the hypoxia probe Pimonidazole at 5 h or 12 h after PFTBA@HSA, PPA@HSA or vehicle treatment; scale bar = 100 μm. **(B-C)** Quantification of relative Pimo+ fluorescence intensity at 5 h or 12 h after treatments (n=3). **(D)** Representative immunofluorescence images of tumor slices stained with the hypoxia probe HIF-1α at 12 h after PFTBA@HSA, PPA@HSA or vehicle treatments; scale bar = 100 μm. **(E)** Quantification of relative HIF-1α fluorescence intensity at 12 h after treatments (n=3). **(F)** Western blot analysis of HIF-1α expression in tumors from vehicle- and PFC@HSAs-treated mice. **(G)** Quantification of Western blot analysis for HIF-1α (n=3). Data are shown as the mean ± SD. Statistical analysis was performed via one-way ANOVA test. *p<0.05; ***p<0.001.

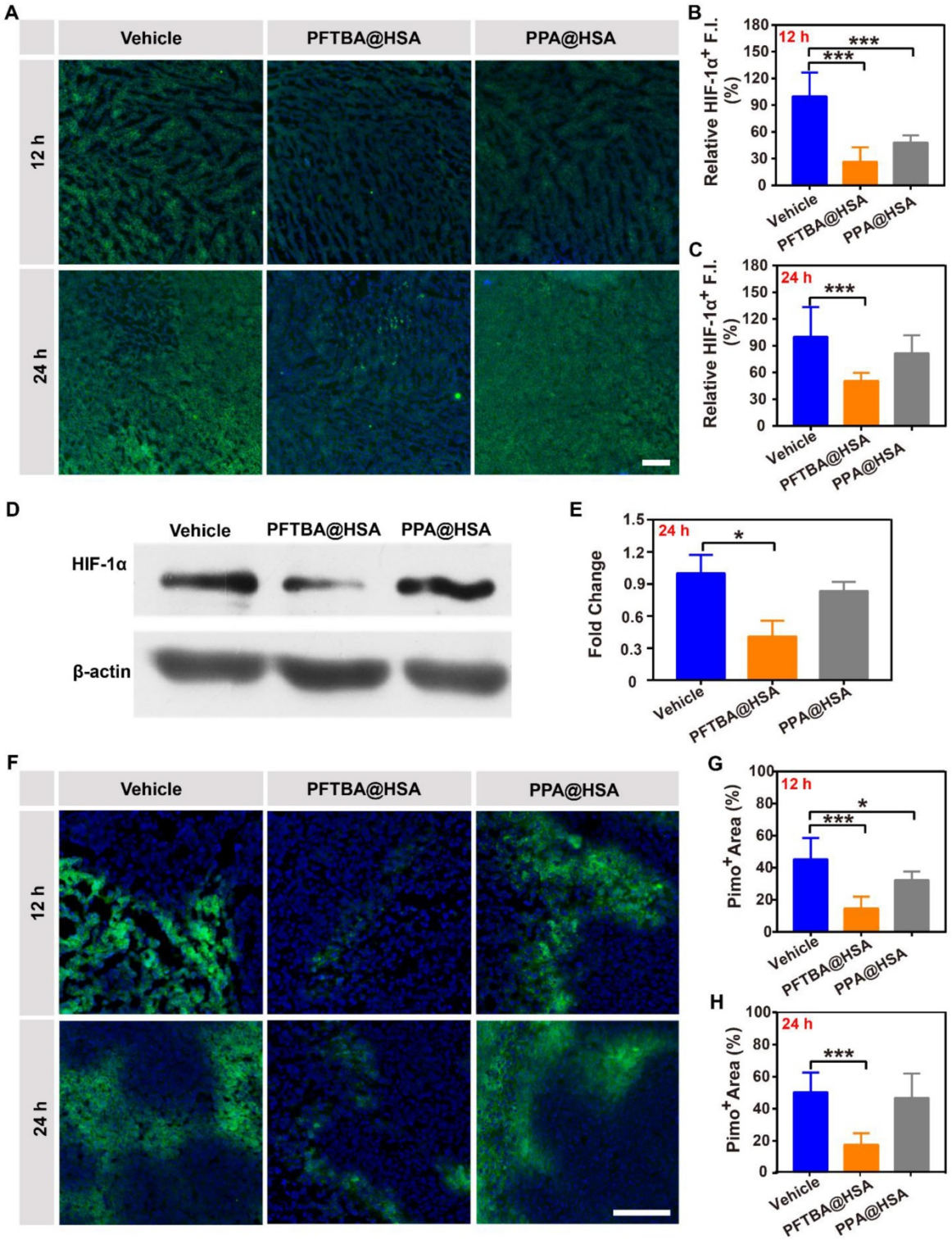

Figure 5. Effects of PFTBA@HSA on relief of CT26 tumor hypoxia after intravenous injection. (A) Representative immunofluorescence images of tumor slices stained with the hypoxia probe HIF-1α at 12 h or 24 h after PFTBA@HSA, PPA@HSA or vehicle treatment; scale bar = 100 μm. **(B-C)** Quantification of relative HIF-1α fluorescence intensity at 12 h or 24 h after treatments (n=3). **(D)** Western blot analysis of HIF-1α expression in tumors from vehicle- and PFC@HSAs-treated mice. **(E)** Quantification of Western blot analysis for HIF-1α (n=3). **(F)** Representative immunofluorescence images of tumor slices stained with the hypoxia indicator Pimonidazole at 12 h or 24 h after PFTBA@HSA, PPA@HSA or vehicle treatment; scale bar = 100 μm. **(G-H)** Quantification of relative Pimo+ fluorescence intensity at 12 h or 24 h after treatments (n=3). Data are shown as the mean ± SD. Statistical analyses were performed via one-way ANOVA test. *p<0.05; ***p<0.001.

Enhanced radiotherapy efficacy of PFTBA@HSA in SUM149PT tumors

Radiotherapy is currently a widely applied cancer therapy strategy in which ionizing radiation is used to induce DNA damage and apoptosis [47, 48]. Tumor hypoxia can significantly limit the formation of stable organic peroxides, causing significantly reduced radiotherapy efficacy [47, 48]. Thus,

PFTBA@HSA could serve as a radiotherapy enhancer by increasing the oxygen supply via two-stage oxygen delivery. The SUM149PT breast tumor model was used to verify this hypothesis. Results showed that PFTBA@HSA itself did not have an effect on tumor growth (**Figure 6A-B**). When PFTBA@HSA was combined with radiotherapy, the tumor growth rate (**Figure 6C-D**) and the tumor weight (**Figure 6F**) were significantly reduced compared to the effects of radiotherapy alone.

Subsequently, H&E staining, TUNEL staining and γH$_2$AX immunological staining were used to evaluate pathological changes in the tumors. The results showed that tumor necrosis and apoptosis were significantly improved by co-treatment of SUM149PT tumors with PFTBA@HSA and radiotherapy (**Figure 6G**). γH$_2$AX immunofluorescence staining was used to evaluate DNA double-strand breaks caused by radiation, and additional DNA double-strand breaks were generated when radiotherapy was co-treated with PFTBA@HSA (**Figure 6G**). Meanwhile, no significant changes in body weight were observed after PFTBA@HSA treatment (**Figure 6E**). Therefore, PFTBA@HSA could be used as a radiotherapy enhancer due to its capacity for two-stage oxygen delivery.

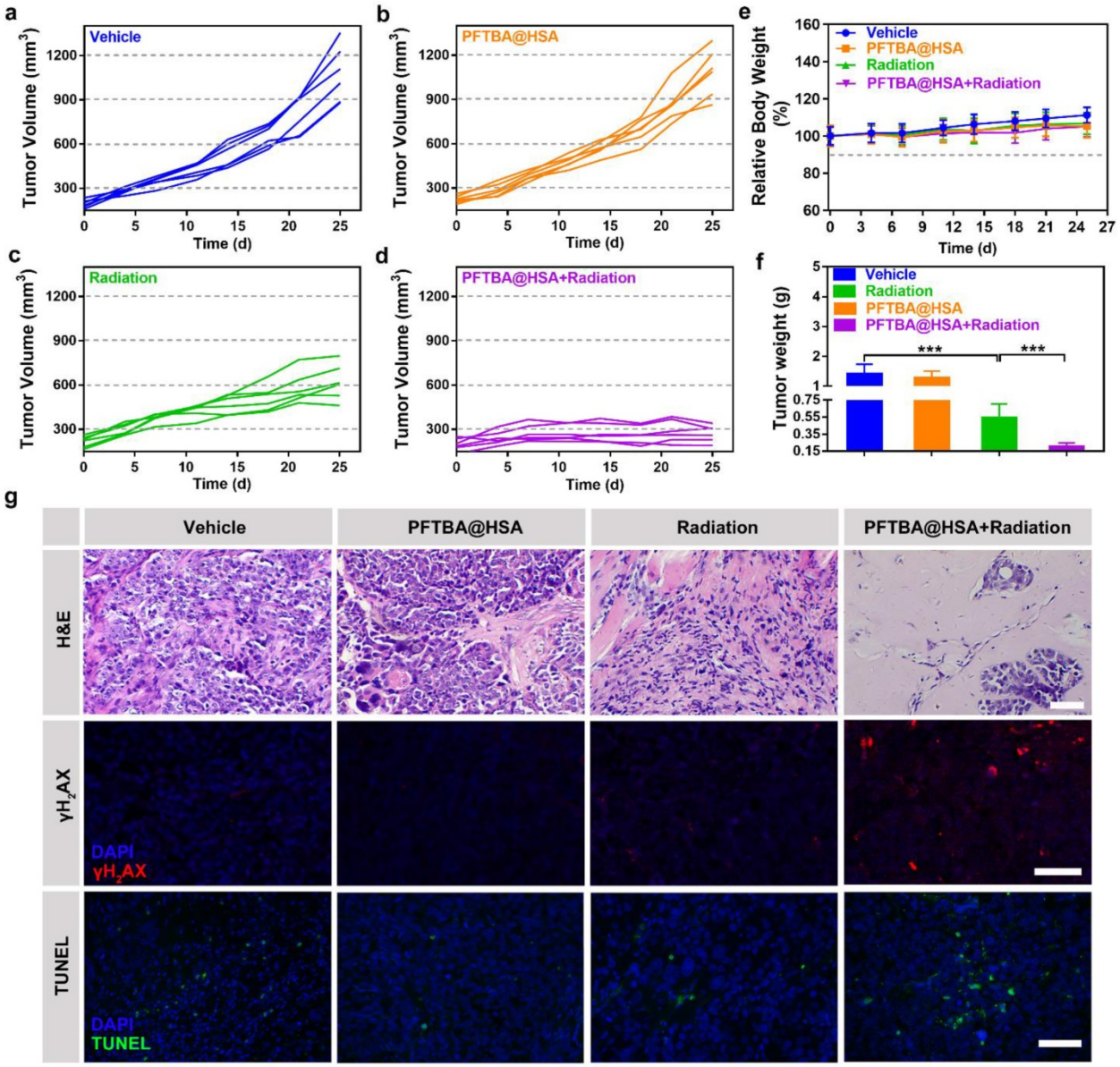

Figure 6. Effects of PFTBA@HSA on radiotherapy in the SUM149PT tumor model. (A-D) Tumor growth curves of SUM149PT tumor-bearing mice after different treatments (n=6). **(E)** Relative mice bodyweight curves (n=6). **(F)** Tumor weight detected at day 25 post-treatments (n=6). **(G)** Representative images of H&E staining, γH$_2$AX staining and TUNEL staining of SUM149PT tumors; scale bar = 50 μm. Data are shown as the mean ± SD. Statistical analyses were performed via one-way ANOVA test. ***p<0.001.

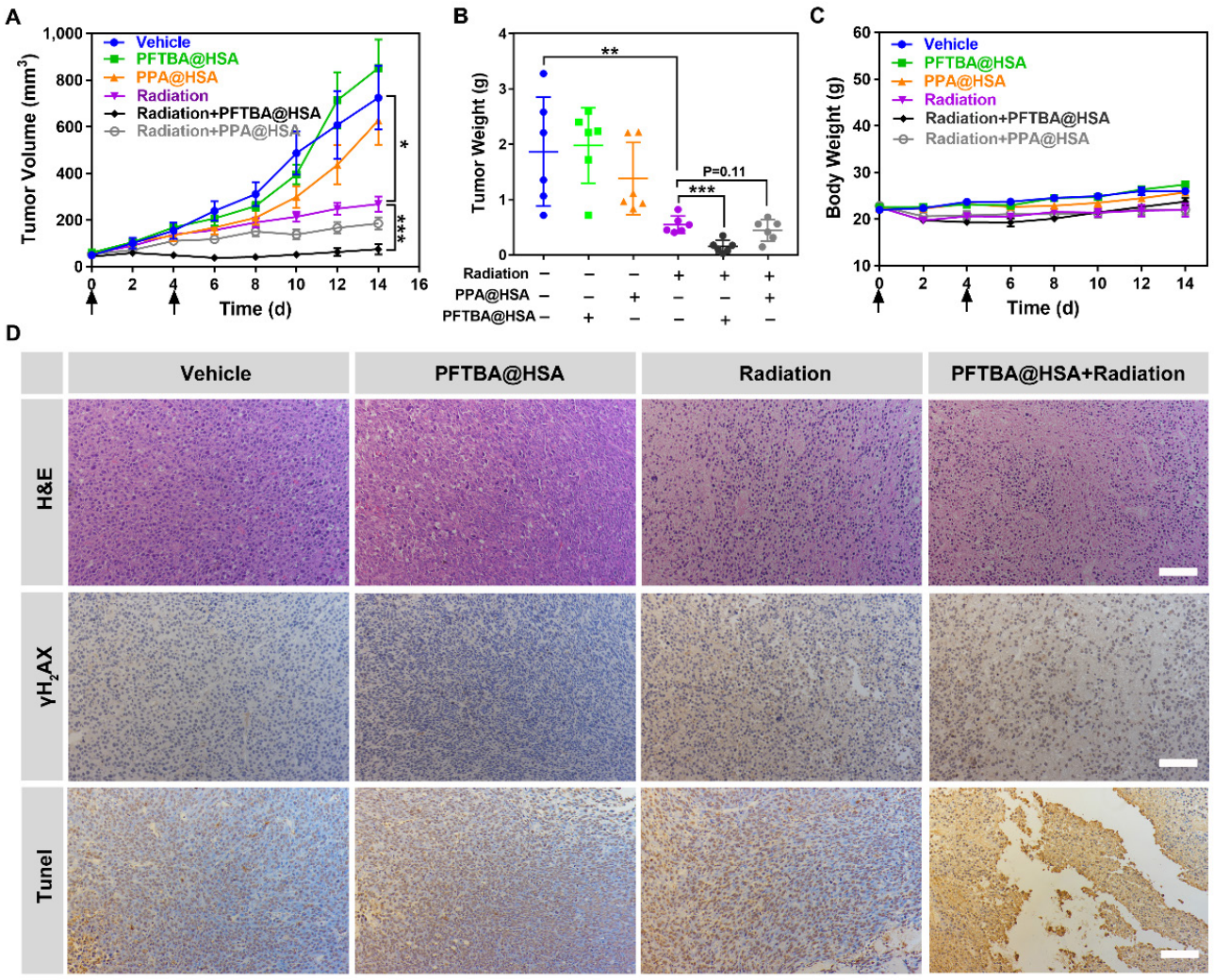

Figure 7. Effects of PFTBA@HSA on radiotherapy in the CT26 tumor model. (A) Tumor growth curves of CT26 tumor-bearing mice post-treatments (n=6). **(B)** Tumor weight detected at the 14th day post-treatments (n=6). **(C)** Mouse bodyweight curves (n=6). **(D)** Representative images of H&E staining, γH2AX staining and TUNEL staining of CT26 tumors; scale bar = 100 μm. Data are shown as the mean ± SD. Statistical analysis were performed via one-way ANOVA test. *p<0.05, **p<0.01, ***p<0.001.

Enhanced radiotherapy efficacy of PFTBA@HSA in more hypoxic CT26 colon tumors

Colon cancer tumors are even more hypoxic than breast cancer tumors [49-51]. The average oxygen partial pressure of normal mammary tissue is 60 mmHg, whereas the average oxygen partial pressure in colon cancer tumors is 30 mmHg [49]. However, in patients with colon cancer, the degree of hypoxia in colon cancer tumor tissue is more obvious, with an average oxygen partial pressure of only approximately 10 mmHg [50, 51]. Therefore, to verify the efficacy of the two-stage PFTBA@HSA oxygen delivery system, a more hypoxic CT26 colon cancer model was chosen to study the radio-sensitization effect of PFTBA@HSA. Results showed that radiotherapy combined with PFTBA@HSA effectively inhibited tumor growth (**Figure 7A**) and reduced tumor weight (**Figure 7B**). Meanwhile, PPA@HSA with only one-stage oxygen delivery could only slightly enhance the efficacy of tumor radiotherapy (P=0.11), meaning that two-stage oxygen delivery may better sensitize radiotherapy than one-stage oxygen delivery. These findings demonstrated that enhanced radiotherapy efficacy could be conferred by PFTBA@HSA compared with the efficacy of radiotherapy alone or PPA@HSA (one-stage oxygen delivery) (**Figure 7A-C**).

Furthermore, some mice were randomly selected and euthanized for tumor collection at 24 h after various treatments. Subsequently, H&E staining and TUNEL and γH2AX immunohistochemical staining were used to assess pathological changes in the tumors. The results showed that tumor cell necrosis, tumor cell apoptosis and the production of DNA double-strand breaks were significantly amplified with PFTBA@HSA and radiotherapy co-treatment (**Figure 7D**). More importantly, no significant changes in bodyweight were noted after PFTBA@HSA

treatment (**Figure 7C**). Taken together, these results suggest that PFTBA@HSA can significantly enhance the sensitivity of CT26 colon cancer to radiotherapy with a high level of biosafety.

In vivo toxicity tests of PFTBA@HSA

The *in vivo* toxicity tests were conducted via normal tissue sections and serum biochemistry analysis. The results showed that PFTBA@HSA possessed no hemolytic effect (**Figure S13**). Moreover, results of H&E staining further confirmed that PFTBA@HSA had no short-term or long-term significant toxicity in normal tissues (**Figure S14-S15**). In addition, the main liver function markers including aspartate aminotransferase (AST) and alanine aminotransferase (ALT) suggested that no obvious influence was found on liver function after PFTBA@HSA treatment (**Figure S16**). The detection of kidney function markers (blood urea nitrogen, BUN and creatinine, Cre) also showed that PFTBA@HSA did not induce obvious toxicity in terms of renal function (**Figure S16**). Thus, PFTBA@HSA possessed good biosafety *in vivo.*

Discussion

Currently, PFCs, a class of chemically inert molecules with good biocompatibility and biosafety, are widely used in the clinic for different purposes, including artificial blood substitution, organ preservation, ultrasound imaging and fluorine magnetic imaging [18-20]. PFCs can actively carry oxygen via physical dissolution at a rate of approximately 20 times that of water and twice that of blood at normal atmospheric pressure [21]. Therefore, PFCs are also widely used as O_2 delivery vehicles. However, the efficacy of PFCs in supplying oxygen to tumors is still insufficient due to the following inherent drawbacks. Generally, PFCs cannot completely release dissolved O_2 even at extremely low partial oxygen pressure due to physical effects [9, 21]. Moreover, during the process of PFC cycling to the tumor, the majority of dissolved oxygen has already been released by simple physical diffusion in the blood, further reducing the O_2 delivery efficiency [9, 21]. Therefore, the usage of PFCs as oxygen suppliers still requires further enhancement.

In this study, we found that PFTBA could significantly increase RBCs infiltration at tumor sites, thereby improving the efficacy of RBCs-mediated O_2 supply. We selected and screened a series of PFCs, including PFTBA, FDC and PPA, among which PFTBA showed the most significant effect on RBCs infiltration. The increased RBCs infiltration at the tumor site combined with the dissolved oxygen characteristics of perfluorocarbon itself formed our two-stage oxygen delivery system. Compared with the one-stage oxygen delivery strategy mediated by the physical oxygen-binding ability of PFC@HSAs, PFTBA@HSA could effectively relieve tumor hypoxia. As a result, tumor hypoxia was efficiently relieved for a long period, which lead to almost entirely inhibited tumor growth after radiotherapy. Our work presents a simple but effective method to reverse the resistance to radiotherapy caused by tumor hypoxia. PFTBA@HSA shows great promise for future clinical translation since all agents, including PFTBA and albumin, are readily available in the clinic and have been verified as nontoxic.

One of the possible mechanisms by which PFTBA increased the vascular permeability of tumors is tumor-targeted platelet inhibition, likely caused by the longest hydrophobic carbon chain of PFTBA. Platelets have recently been shown to play a crucial role in the maintenance of tumor vessel integrity by secreting active ingredients, such as serotonin, angiogenin-1 and transforming growth factors [44, 52-54]. These active ingredients can effectively increase endothelial cell numbers, optimize endothelial cell arrangements and increase endothelial cell tight junctions [44, 52-54]. Thus, PFTBA can improve the vascular permeability of tumors via targeted platelet inhibition, leading to significantly increased RBCs penetration and enhanced cell oxygenation at the tumor site. In this study, PFTBA was encapsulated in albumin to form nanoparticles, which accumulated in tumor tissue via the EPR effect. In addition, PFTBA@HSA actively accumulated at the tumor site due to the high affinity between albumin and highly expressed SPARC on the tumor surface. Finally, PFTBA accumulated at the tumor site selectively inhibited platelets in the tumor to improve tumor vascular permeability and O_2 supply.

On the other hand, platelets also play a vital role in promoting tumor metastasis.[55, 56] Platelets can actively combine with circulating tumor cells to form tumor thrombi that are able to avoid the damage induced by blood shear force and natural killer cell recognition and killing, ultimately enhancing tumor cell survival in the blood [55]. At the same time, ATP released by activated platelets can significantly enhance the penetration and infiltration of tumor cells at distant metastasis sites [56]. Currently, platelet inhibition has already been shown to be the most efficient way to inhibit tumor metastasis [57]. Therefore, we speculate that the two-stage oxygen delivery system designed in this study can further inhibit tumor metastasis. To confirm this hypothesis, we preliminarily studied the anti-tumor metastasis ability of PFTBA@HSA in 4T1 tumors. The results

showed that the number of 4T1 tumor lung metastases was 5.6±2.4 after PFTBA@HSA treatment, whereas the number in the blank group was 23.2±8.70, indicating that PFTBA@HSA inhibited *in situ* tumor metastasis through effective platelet inhibition (**Figure S17-S18**).

Recently, platelet inhibition has also been demonstrated to be an effective approach for sensitizing tumors to immunotherapy [58]. Platelets can activate latent TGF-β through the GARP protein on their surface [58, 59], and increased TGF-β activation can significantly inhibit T cell activity [60]. Through platelet inhibition, the amount of activated TGF-β in the blood can be significantly reduced, thereby enhancing the effect of T-cell immunotherapy [58]. Therefore, we speculate that PFTBA can also effectively increase T-cell activity through platelet inhibition to sensitize tumors to immunotherapy (**Figure S19**).

Conclusion

In this study, we found that PFTBA could increase RBCs infiltration and O_2 delivery via physically dissolved oxygen. Then, we established a two-stage O_2 delivery system using PFTBA as oxygen carrier and albumin as PFTBA carrier. The tumor growth rate in response to radiotherapy of breast cancer (SUM149PT) decreased from 40% to 14% when compared with the vehicle after application of the two-stage oxygen delivery system. For the more hypoxic colon cancer (CT26), the tumor growth rate also decreased from 30% to 15%. Our work provides a simple but effective method to reverse tumor hypoxia and thus reverse tumor resistance to radiotherapy. PFTBA@HSA shows great promise for future clinical transition since all agents, including PFTBA and albumin, are readily available in the clinic and have been verified as nontoxic.

Abbreviations

ALT: alanine aminotransferase; AST: aspartate aminotransferase; BUN: blood urea nitrogen; CRE: creatinine; EPR: enhanced permeability and retention; FDC: perfluorodecalin; HSA: human serum albumin; PFC: perfluorocarbon; PFTBA: perfluorotributyl-amine; PPA: perfluorotripropylamine; PRP: platelet-rich plasma; RBC: red blood cell; SPARC: secreted protein acidic and rich in cysteine; TEM: transmission electron microscopy.

Supplementary Material

Supplementary methods and figures.
http://www.thno.org/v08p4898s1.pdf

Acknowledgements

This paper was supported by National Key R&D Program of China (2017YFA0205400); National Natural Science Foundation of China (No. 81202474, 81273464, 81473146, 81872811, 31872755); Natural Science Foundation of Jiangsu BE2015674; Changzhou Special Project of Biotechnology and Biopharmacy (No. CE20105006).

Competing Interests

The authors have declared that no competing interest exists.

References

1. Harris AL. Hypoxia - a key regulatory factor in tumour growth. Nat Rev Cancer. 2002; 2: 38-47.
2. Vaupel P, Mayer A. Hypoxia in cancer: Significance and impact on clinical outcome. Cancer Metastasis Rev. 2007; 26: 225-39.
3. Dewhirst MW, Cao YT, Moeller B. Cycling hypoxia and free radicals regulate angiogenesis and radiotherapy response. Nat Rev Cancer. 2008; 8:425–37.
4. Schaue D, McBride WH. Opportunities and challenges of radiotherapy for treating cancer. Nat Rev Clin Oncol. 2015; 12: 527-40.
5. Fan WP, Bu WB, Shen B, He QJ, Cui ZW, Liu YY, et al. Intelligent MnO_2 nanosheets anchored with upconversion nanoprobes for concurrent ph-/H_2O_2-responsive ucl imaging and oxygen-elevated synergetic therapy. Adv Mater. 2015; 27: 4155-61.
6. Fan WP, Bu WB, Zhang Z, Shen B, Zhang H, He QJ, et al. X-ray radiation-controlled no-release for on-demand depth-independent hypoxic radiosensitization. Angew Chem Int Ed. 2015; 54: 14026-30.
7. Zhang C, Zhao KL, Bu WB, Ni DL, Liu YY, Feng JW, et al. Marriage of scintillator and semiconductor for synchronous radiotherapy and deep photodynamic therapy with diminished oxygen dependence. Angew Chem Int Ed. 2015; 54: 1770-74.
8. Saugstad OD. Hyperoxia in the term newborn: More evidence is still needed for optimal oxygen therapy. Acta Paediatr. 2012; 101: 34-38.
9. Song X, Feng L, Liang C, Yang K, Liu Z. Ultrasound triggered tumor oxygenation with oxygen-shuttle nanoperfluorocarbon to overcome hypoxia-associated resistance in cancer therapies. Nano Lett. 2016; 16: 6145-53.
10. Alayash AI. Mechanisms of toxicity and modulation of hemoglobin-based oxygen carriers (HBOCs). Shock. 2017.
11. Lee NP, Chan KT, Choi MY, Lam HY, Tung LN, Tzang FC, et al. Oxygen carrier YQ23 can enhance the chemotherapeutic drug responses of chemoresistant esophageal tumor xenografts. Cancer Chemother Pharmacol. 2015; 76: 1199-207.
12. Meng LT, Cheng YL, Gan SJ, Zhang ZC, Tong XN, Xu L, et al. Facile deposition of manganese dioxide to albumin-bound paclitaxel nanoparticles for modulation of hypoxic tumor microenvironment to improve chemoradiation therapy. Mol Pharm. 2018; 15: 447-57.
13. Song XJ, Feng LZ, Liang C, Yang K, Liu Z. Ultrasound triggered tumor oxygenation with oxygen-shuttle nanoperfluorocarbon to overcome hypoxia-associated resistance in cancer therapies. Nano Lett. 2016; 16: 6145-53.
14. Gong H, Chao Y, Xiang J, Han X, Song G, Feng L, et al. Hyaluronidase to enhance nanoparticle-based photodynamic tumor therapy. Nano Lett. 2016; 16: 2512-21.
15. Mazzone M, Dettori D, de Oliveira RL, Loges S, Schmidt T, Jonckx B, et al. Heterozygous deficiency of PHD2 restores tumor oxygenation and inhibits metastasis via endothelial normalization. Cell. 2009; 136: 839-51.
16. Rivera LB, Bergers G. Tumor angiogenesis, from foe to friend. Science. 2015; 349: 694-95.
17. Paez-Ribes M, Allen E, Hudock J, Takeda T, Okuyama H, Vinals F, et al. Antiangiogenic therapy elicits malignant progression of tumors to increased local invasion and distant metastasis. Cancer cell. 2009; 15: 220-31.
18. Zhou Y, Wang ZG, Chen Y, Shen HX, Luo ZC, Li A, et al. Microbubbles from gas-generating perfluorohexane nanoemulsions for targeted temperature-sensitive ultrasonography and synergistic hifu ablation of tumors. Adv Mater. 2013; 25: 4123-30.
19. Schutt EG, Klein DH, Mattrey RM, Riess JG. Injectable microbubbles as contrast agents for diagnostic ultrasound imaging: The key role of perfluorochemicals. Angew Chem Int Ed. 2003; 42: 3218-35.
20. Riess JG. Oxygen carriers ("blood substitutes") - raison d'etre, chemistry, and some physiology. Chem Rev. 2001; 101: 2797-919.
21. Castro CI, Briceno JC. Perfluorocarbon-based oxygen carriers: Review of products and trials. Artif Organs. 2010; 34: 622-34.
22. Song GS, Liang C, Yi X, Zhao Q, Cheng L, Yang K, et al. Perfluorocarbon-loaded hollow Bi_2Se_3 nanoparticles for timely supply of

oxygen under near-infrared light to enhance the radiotherapy of cancer. Adv Mater. 2016; 28: 2716-23.
23. Gao M, Liang C, Song XJ, Chen Q, Jin QT, Wang C, et al. Erythrocyte-membrane-enveloped perfluorocarbon as nanoscale artificial red blood cells to relieve tumor hypoxia and enhance cancer radiotherapy. Adv Mater. 2017; 29(35): 1701429.
24. Chen J, Luo HL, Liu Y, Zhang W, Li HX, Luo T, et al. Oxygen-self-produced nanoplatform for relieving hypoxia and breaking resistance to sonodynamic treatment of pancreatic cancer. ACS Nano. 2017; 11: 12849-62.
25. Zhang K, Xu HX, Jia XQ, Chen Y, Ma M, Sun LP, et al. Ultrasound-triggered nitric oxide release platform based on energy transformation for targeted inhibition of pancreatic tumor. ACS Nano. 2016; 10: 10816-28.
26. Zhang K, Xu HX, Chen HR, Jia XQ, Zheng SG, Cai XJ, et al. CO_2 bubbling-based 'nanobomb' system for targetedly suppressing panc-1 pancreatic tumor via low intensity ultrasound-activated inertial cavitation. Theranostics. 2015; 5: 1291-302.
27. Zhang K, Chen HR, Li FQ, Wang Q, Zheng SG, Xu HX, et al. A continuous tri-phase transition effect for HIFU-mediated intravenous drug delivery. Biomaterials. 2014; 35: 5875-85.
28. Kimura H, Braun RD, Ong ET, Hsu R, Secomb TW, Papahadjopoulos D, et al. Fluctuations in red cell flux in tumor microvessels can lead to transient hypoxia and reoxygenation in tumor parenchyma. Cancer Res. 1996; 56: 5522-8.
29. Ho-Tin-Noe B, Goerge T, Cifuni SM, Duerschmied D, Wagner DD. Platelet granule secretion continuously prevents intratumor hemorrhage. Cancer Res. 2008; 68: 6851-8.
30. Li SP, Zhang YL, Wang J, Zhao Y, Ji TJ, Zhao X, et al. Nanoparticle-mediated local depletion of tumour-associated platelets disrupts vascular barriers and augments drug accumulation in tumours. Nat Biomed Eng. 2017; 1: 680-692.
31. Li R, Ren MP, Chen N, Luo M, Deng X, Xia JY, et al. Presence of intratumoral platelets is associated with tumor vessel structure and metastasis. BMC Cancer. 2014; 14(1): 167.
32. Jiang C, Cheng H, Yuan A, Tang X, Wu J, Hu Y. Hydrophobic IR780 encapsulated in biodegradable human serum albumin nanoparticles for photothermal and photodynamic therapy. Acta Biomater. 2015; 14: 61-9.
33. Zhang YF, He LY, Wu J, Wang KK, Wang J, Dai WM, et al. Switchable pdt for reducing skin photosensitization by a NIR dye inducing self-assembled and photo-disassembled nanoparticles. Biomaterials. 2016; 107: 23-32.
34. Zhang K, Li P, He YP, Bo XW, Li XL, Li DD, et al. Synergistic retention strategy of RGD active targeting and radiofrequency-enhanced permeability for intensified RF & chemotherapy synergistic tumor treatment. Biomaterials. 2016; 99: 34-46.
35. Zhang K, Li P, Chen HR, Bo XW, Li XL, Xu HX. Continuous cavitation designed for enhancing radiofrequency ablation via a special radiofrequency solidoid vaporization process. ACS Nano. 2016; 10: 2549-58.
36. Nachman RL, Rafii S. Platelets, petechiae, and preservation of the vascular wall. N Engl J Med. 2008; 359: 1261-70.
37. Wagner DD. How platelets safeguard vascular integrity. J Thromb Haemost. 2011; 9: 56-65.
38. Ho-Tin-Noe B, Goerge T, Wagner DD. Platelets: Guardians of tumor vasculature. Cancer research. 2009; 69: 5623-6.
39. Pidcoke HF, Shade RE, Herzig MC, Schaffer BS, Fedyk CG, Prat N, et al. A third generation perfluorocarbon causes thrombocytopenia, platelet dysfunction and changes in blood morphology in a baboon model of systemic inflammation. Blood. 2013; 122:2327.
40. Lowe KC. Second-generation perfluorocarbon emulsion blood substitutes. Artif Cells Blood Substit Immobil Biotechnol. 2000; 28: 25-38.
41. Tuliani VV, Orear EA, Fung BM, Sierra BD. Interaction between erythrocytes and a perfluorochemical blood substitute. J Biomed Mater Res. 1988; 22: 45-61.
42. Saba S, Mason R. Effects of platelets and certain platelet components on growth of cultured human endothelial cells. Thromb Res. 1975; 7: 807-12.
43. Sabrkhany S, Griffioen AW, oude Egbrink MG. The role of blood platelets in tumor angiogenesis. BBA-Reviews on Cancer. 2011; 1815: 189-96.
44. HO-TIN-NOÉ B, Demers M, Wagner DD. How platelets safeguard vascular integrity. J Thromb Thrombolysis. 2011; 9: 56-65.
45. Spahn DR. Blood substitutes artificial oxygen carriers: Perfluorocarbon emulsions. Crit Care. 1999; 3: R93-R7.
46. Riess JG. Perfluorocarbon-based oxygen delivery. Artif Cell Blood Sub. 2006; 34: 567-80.
47. Song GS, Chen YY, Liang C, Yi X, Liu JJ, Sun XQ, et al. Catalase-loaded taox nanoshells as bio-nanoreactors combining high-z element and enzyme delivery for enhancing radiotherapy. Adv Mater. 2016; 28: 7143-8.
48. Song GS, Ji CH, Liang C, Song XJ, Yi X, Dong ZL, et al. Taox decorated perfluorocarbon nanodroplets as oxygen reservoirs to overcome tumor hypoxia and enhance cancer radiotherapy. Biomaterials. 2017; 112: 257-63.
49. Vaupel P, Schlenger K, Knoop C, Hockel M. Oxygenation of human tumors-evaluation of tissue oxygen distribution in breast cancers by computerized O_2 tension measurements. Cancer Res. 1991; 51: 3316-22.
50. Zhang LR, Hu Y, Xi N, Song J, Huang WJ, Song SS, et al. Partial oxygen pressure affects the expression of prognostic biomarkers Hif-1 alpha, Ki67, and CK20 in the microenvironment of colorectal cancer tissue. Oxid Med Cell Longev. 2016; 1204715.
51. Burmakin M, van Wieringen T, Olsson PO, Stuhr L, Ahgren A, Heldin CH, et al. Imatinib increases oxygen delivery in extracellular matrix-rich but not in matrix-poor experimental carcinoma. J Transl Med. 2017; 15.
52. Ho-Tin-Noe B, Goerge T, Cifuni SM, Duerschmied D, Wagner DD. Platelet granule secretion continuously prevents intratumor hemorrhage. Cancer Res. 2008; 68: 6851-8.
53. Furie B, Furie BC. Mechanisms of thrombus formation. N Engl J Med. 2008; 359: 938-49.
54. Kisucka J, Butterfield CE, Duda DG, Eichenberger SC, Saffaripour S, Ware J, et al. Platelets and platelet adhesion support angiogenesis while preventing excessive hemorrhage. Proc Natl Acad Sci U S A. 2006; 103: 855-60.
55. Valastyan S, Weinberg RA. Tumor metastasis: Molecular insights and evolving paradigms. Cell. 2011; 147: 275-92.
56. Schumacher D, Strilic B, Sivaraj KK, Wettschureck N, Offermanns S. Platelet-derived nucleotides promote tumor-cell transendothelial migration and metastasis via $P2Y_2$ receptor. Cancer Cell. 2013; 24: 130-7.
57. Zhang Y, Wei J, Liu S, Wang J, Han X, Qin H, et al. Inhibition of platelet function using liposomal nanoparticles blocks tumor metastasis. Theranostics. 2017; 7: 1062-71.
58. Rachidi S, Metelli A, Riesenberg B, Wu BX, Nelson MH, Wallace C, et al. Platelets subvert T cell immunity against cancer via GARP-TGFβ axis. Sci Immunol. 2017; 2(11).
59. Wallace CH, Wu BX, Salem M, Ansa-Addo EA, Metelli A, Sun S, et al. B lymphocytes confer immune tolerance via cell surface GARP-TGF-β complex. JCI Insight. 2018; 3(7).
60. Metelli A, Wu BX, Fugle CW, Rachidi S, Sun S, Zhang Y, et al. Surface expression of tgfbeta docking receptor GARP promotes oncogenesis and immune tolerance in breast cancer. Cancer Res. 2016; 76: 7106-17.